ELSEVIER

Comput. Methods Appl. Mech. Engrg. 145 (1997) 147–166

Computer methods in applied mechanics and engineering

Passive and active design of hard disk suspension assemblies using multiobjective optimization techniques

Yee-Pien Yang*, Chin-Chung Kuo

Department of Mechanical Engineering, National Taiwan University, Taipei, Taiwan 106, ROC

Received 9 June 1996; revised 9 Sepember 1996

Abstract

The passive and active system designs for hard disk suspension assemblies are formulated as multiobjective optimization problems. The maximization of natural frequencies is treated as a set of objectives in the passive design, subject to side constraints on the design variables that describe the dimensions of the suspension system. The active design integrates both structural and control objectives, and is characterized by a set of objective natural frequencies and an optimal control performance index with weighted system state regulation errors and control efforts. Preloading and air bearing effects are both considered in the optimal design. An interface program is used to communicate between the finite element analyzer and the optimizer using the multiobjective optimization techniques of goal programming and compromise programming. The feasibility of the optimal design is demonstrated and the frequency responses of the proposed designs are investigated.

1. Introduction

Current magnetic hard disk drives are small, light-weight and have high-area recording density as well as fast and accurate data access. Disk drives have been developed with close to head-disk contact with flying heights of less than 0.02 μm, and with recording densities over 3×10^8 bit/in^2 [1]. Since the flying height is observed to oscillate at a very small amplitude, excessive vibration induced by disturbances can cause catastrophic damage to the hard disk system. Major sources of disturbances include disk surface roughness, fast seek motion, vibrations from the actuator arm, spindle/bearing misalignment, rotating flow around the suspension, and so on [2–4].

It is quite intuitive and natural for the design objectives to raise the natural frequencies of the suspension assembly so that it is not easily excited by undesirable disturbances. There exist two classes of strategy for structure optimization with frequency requirements. Either the weight of the structure is minimized subject to frequency constraints, or the frequencies are maximized subject to the constraint on the shape, weight or frequency distributions. Many designers minimize the structure weight with frequency constraints [5–7]. In this strategy, scaling procedures are required to adjust frequencies after each iteration to the level specified by the constraints [8]. Therefore, difficulties would arise if the element stiffness matrices are nonlinear in terms of design variables or multiple frequencies are involved.

Other researchers have treated natural frequencies as objective functions. Szyszkowski [9] presented a method for the optimization of the maximum frequency of free vibrations, handling structures which might experience multimodal eigen-solutions during the solution phase. Szyszkowski and King [6] derived optimality criteria to

* Corresponding author.

PII S0045-7825(96)01188-7

maximize a set of frequencies for a structure of a given weight. An error norm was proposed and used to determine the optimum values of design variables and Lagrange multipliers.

In recent years, the control performance and control effort have been considered simultaneously with structure optimization, resulting in an integrated structure and control optimization technology. This technology optimizes not only the weight or natural frequencies of a structure, but also improves the closed-loop frequency response. Various multiobjective optimization techniques have been proposed and applied in the industry. For application to the combined structure/control optimization problem, Livne et al. [10] formulated the synthesis of an actively controlled composite wing as a multidisciplinary optimization problem, where a unique integration of analysis techniques spanning the disciplines of structures, aerodynamics, and controls is described. Gilbert and Schmidt [11] proposed a multilevel optimization approach to the integrated structure/control law design. The lower level consisted of an independent structural design and control law design, the design results and sensitivities were coordinated through an upper level optimization problem that reflected the desired objectives of the integrated structure/control law design. Rao [12] also presented a general methodology for the multiobjective optimization of actively controlled structures, in which the fuzzy set and game theories were combined.

This paper extends the state-of-the-art in multiobjective optimization design to the suspension assemblies. First, the passive structure optimization is investigated so that the natural frequencies of the suspension are maximized, subject to some side constraints on the design variables of the suspension assembly. Second, the integrated structure and control optimization is applied to the actively controlled suspension assemblies, where the performance index of the linear quadratic regulator is incorporated with frequency objectives. Moreover, the controllability of the bending and torsional modes is guaranteed by two independent control forces, which can be implemented by piezoelectric actuators.

2. Modeling of suspension assembly

The hard disk suspension assembly consists of a mounting block, suspension beam, flexure and slider. Fig. 1 shows an unloaded suspension of the Hutchinson Type 870 used in this research. The suspension is connected with the mounting block by eight weld points. The slider is attached on the flexure with epoxy adhesive in the shaded area. The flexure is attached to the suspension beam by four diamond shaped weld points. The slider and the suspension beam are separated by a hemispherical flexure knob so that the slider is able to perform pitch and roll motions in its operation mode, and the sliding motion is prohibited by the contact friction. The dimensions of each part of the suspension assembly are listed in Appendix A.

The finite element model is created with the undeformed state of suspension. After being loaded onto the hard disk, the suspension undergoes a preloading force of about 5.5269 N, causing the angle between the suspension and the base line of the mounting block to reduce from 10 to about 2 degrees. The lift clearance is approximately 2 mm measured at the front tip of the slider, and is about 1.5 mm at the back tip, in the vertical direction. This loading process can be performed using the analysis procedures of ABAQUS[1]. In the ABAQUS program, the user simply divides the loading histories into *steps* and comes up with the deformed state of pre-stress for subsequent analyses.

The air bearing that separates the slider from the media during the operation is approximated by four linear springs providing support at the four corners of the slider. Since the flying height at the front corners of the slider is higher than that at the rear corners, the stiffness of each front corner is modeled by 1×10^5 Nt/m, while the stiffness of each rear corner is 1.5×10^5 Nt/m. The corresponding flying height is around 0.225 μm under a load force about 0.012 kg, according to the previous experiments on the measurement of flying height [13].

2.1. Finite element model

The finite element model for the suspension assembly initially includes a grand total of 338 elements, 439

[1] ABAQUS is a registered trademark of Hibbit, Karlsson and Dorensen, Inc.

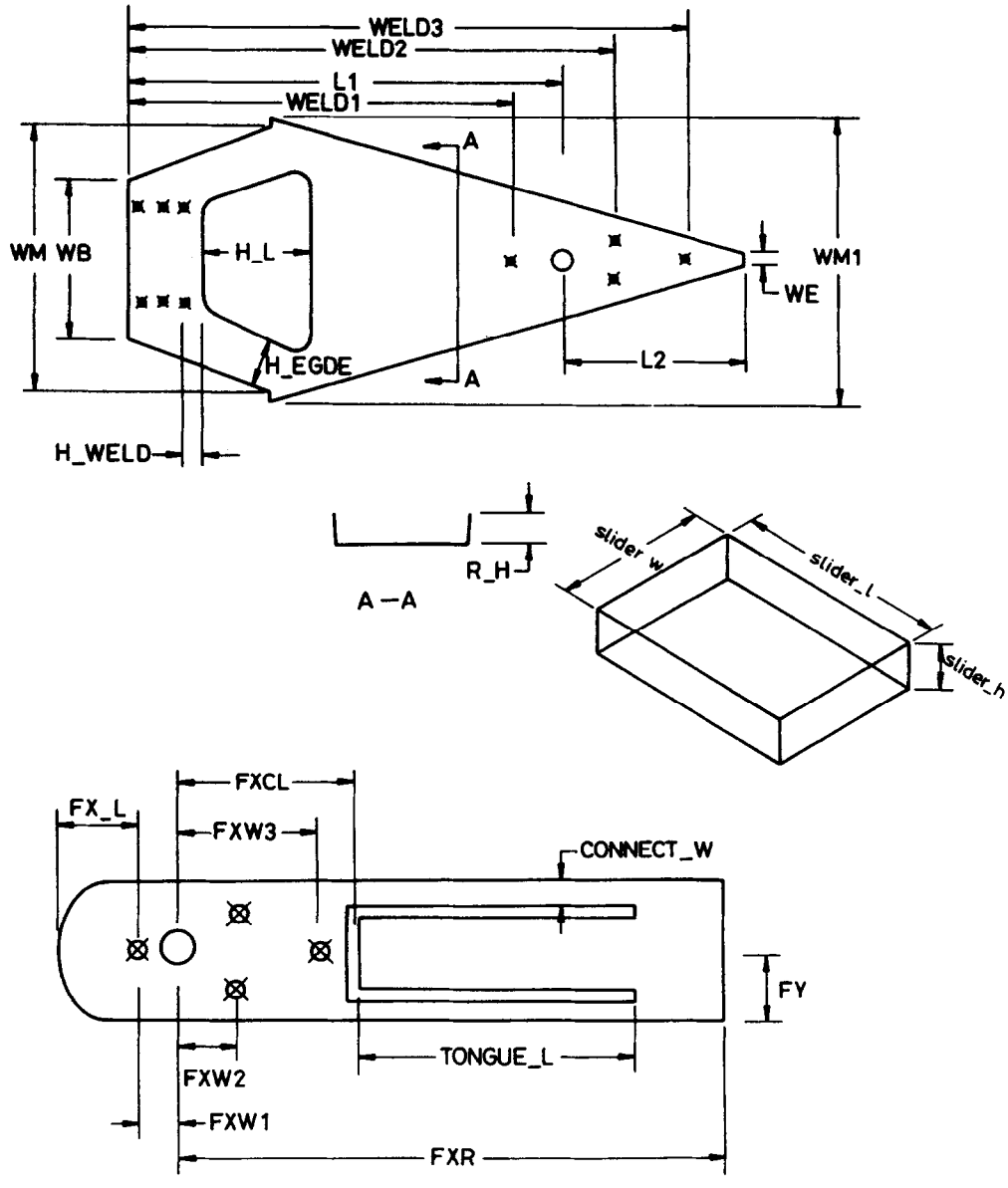

Fig. 1. Unloaded suspension of the Hutchinson Type 870.

nodes, with 2551 degrees of freedom. It should be noted that the mesh number is automatically adjusted according to the updated values of design variables obtained by the iterative search of the optimizer. Two types of elements are used: for the suspension and flexure, we use the quadrilateral thin shell element (S4R5) of 4 nodes, each of which includes 3 orthogonal displacements and two rotations along the shell plane. For the slider, the 8-node linear brick (C3D8) is used, incompressible and hybrid with 3 displacement degrees of freedom for each node. The mounting block is regarded as a fixed rigid body, to which the suspension beam is connected with weld points.

The mesh generation subroutine defines nodal coordinates as functions of design variables. Three shape parameters are selected as design variables:

H_{BASE}: distance between the left edge of the hole and the mounting block

H_L: length of the hole

R_H: height of the suspension flaps

Other parameters are left constants, including the thickness, tip width and total length of the suspension, the distance of the side-edge of the hole and the rim of the suspension, and the sizes of flexure and slider. The reasons why we do not choose all the above parameters as design variables are explained in the following section on sensitivity analysis. The finite element models of the suspension assembly as well as its components are shown in Fig. 2.

A model of nine nodes, located at $X0$, that are not welded but supported on the mounting block are shown in

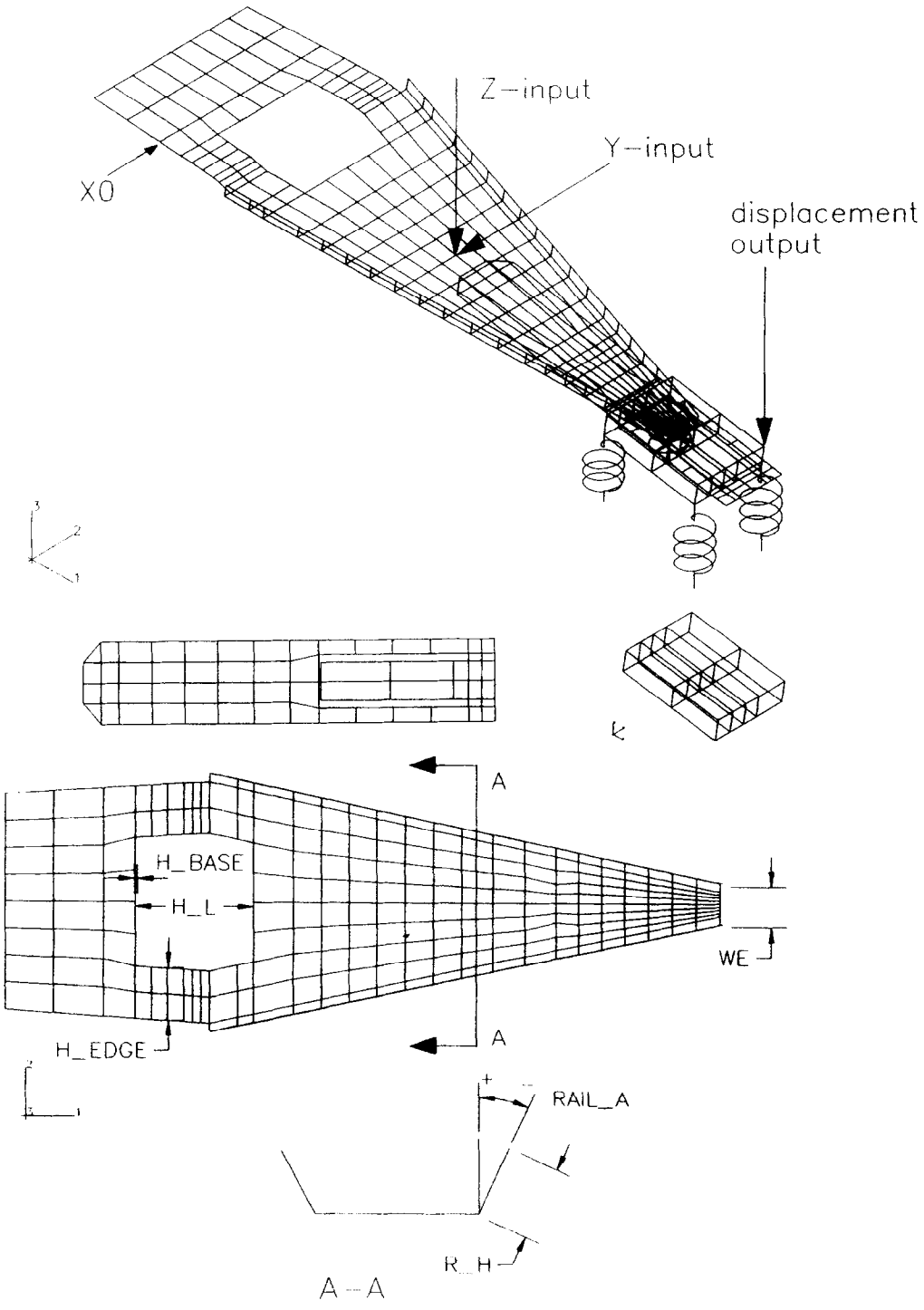

Fig. 2. Finite element model of suspension assembly.

Fig. 2. Accordingly, seven inner nodes are restrained in their three rotational degrees of freedom, while two edge nodes are left free. All the weld points between the suspension and flexure are compatible and are modeled as the same nodes with the same six degrees of freedom. The contact point of the pivot knob between the suspension and flexure is modeled as a contacting node, whose displacements in the y- and z-directions are identically restrained in both component directions. However, the displacements of the contacting nodes in the x-direction are independent; i.e. the knob is allowed to slide freely on the suspension in the x-direction.

2.2. Dynamical model and preload process

The equations of motion of the suspension assembly for the finite element model of order N have the form

$$M(x)\ddot{q} + C(x)\dot{q} + K(x)q = Bu \tag{1}$$

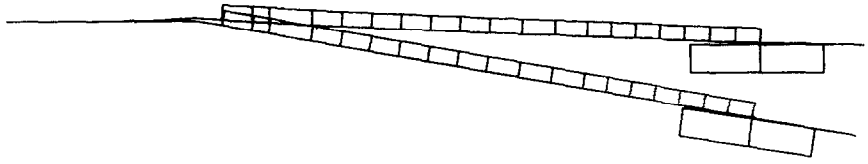

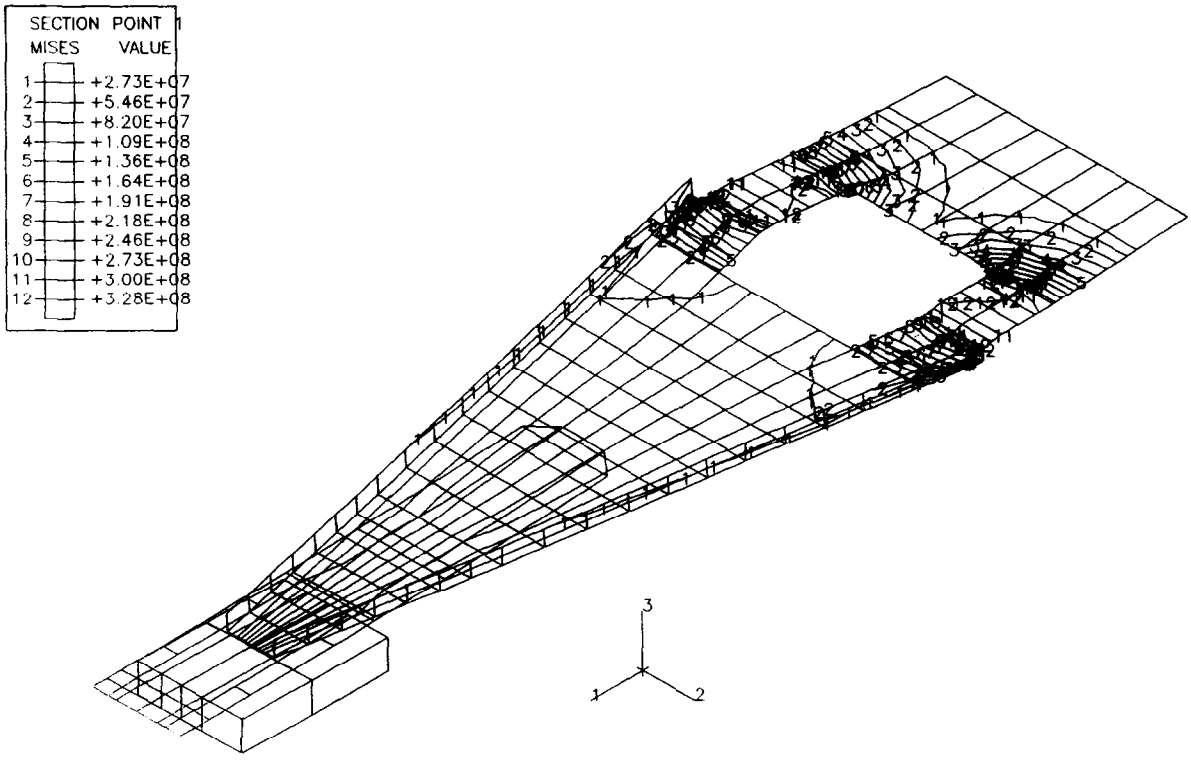

Fig. 3. (a) Loading process; (b) pre-stress distribution in the loaded state of suspension assembly.

Table 1
Natural frequencies of suspension assembly (Unit: Hz)

Mode	Unloaded		Loaded	
	Frequency	Type	Frequency	Type
1	2282	bending	2241	bending
2	2606	torsional	2770	torsional
3	5732	torsional	6813	bending
4	6668	bending	6974	torsional

where $\boldsymbol{x}$ is a vector of design variables, $M(\boldsymbol{x})$ is a positive definite symmetric mass matrix, $K(\boldsymbol{x})$ is the nonnegative symmetric stiffness matrix, including the equivalent stiffness due to the preload produced pre-stress and pre-strain, and $\boldsymbol{q}$ is the vector of the generalized nodal coordinates. In the modal analysis during the optimization process, the input $\boldsymbol{u}$, its influence matrix B, and the damping matrix $C(\boldsymbol{x})$ are neglected while searching for natural frequencies and natural modes of the system. Once we obtain the optimal design of the suspension assembly, the modal damping ratios are included in the modal equations so that more analyses, such as time responses, vibration controls, etc. can be performed. In the simulation, the damping ratio is chosen at 0.0001 for each mode.

Since the optimization process is performed with the suspension assembly in its loaded status, a large deformation occurs in the loading process of the suspension onto the hard disk, resulting in a nonlinear problem formulation. The modeling of the preloading process is accomplished by a feature of 'step' defined as a portion of the analysis history in ABAQUS. ABAQUS uses iterations of Newton's method to obtain the loaded state of the suspension with pre-stress and pre-strain distributions in the finite element model. Fig. 3 describes the loading process and pre-stress distribution of the suspension assembly. This model is used in the subsequent dynamical analysis for each optimization loop.

The first 4 natural frequencies of the original suspension in the unloaded and loaded positions are compared in Table 1. Due to the preload induced pre-strain and pre-stress in the suspension beam, the first bending natural frequency is smaller than that of the unloaded beam. However, the first torsional frequency of the loaded suspension is higher than that in the unloaded condition. This is a result of the vertical constraints caused by the preload increase in torsional stiffness. It is also found that the third mode under preload becomes a bending mode. This is possibly due to the vertical preload making it easier for the bending vibration of the loaded suspension to be compressed in a bending shape.

3. Multiobjective optimization design

3.1. Passive structure design and objectives

From the modal analysis of the suspension assembly, the first bending and torsional mode frequently occur in the following way: the first mode is a bending mode and the second torsional; or the first mode is a torsional mode and the second bending [14]. Other types of modal sequence rarely occur. However, the third mode may be a bending, torsional or a hybrid of these modes. Therefore, the objectives of the optimization of suspension assembly are as follows:

(1) Design the natural frequencies of the first bending and torsional modes as high as possible so that they are not easily excited by disturbances, such as the 60 Hz disk rotation speed and its harmonics [13], and the air-flow between disks [4].
(2) Separate the second and the third natural frequencies take apart as far as possible to reduce the likelihood that both of these modes will be excited simultaneously.

The above two objectives interfere with each other. The farther the second and the third natural frequencies are separated, the lower the first natural frequency. Multiobjective optimization techniques will compromise those objectives that conflict and produce a satisfactory optimal design [15,16].

The multiobjective optimization problem can be stated as follows:

Minimize the cost functionals

$$f_1 = \frac{1}{\omega_1} \tag{2}$$

$$f_2 = \frac{1}{\omega_2} \tag{3}$$

$$f_3 = \frac{1}{\omega_3 - \omega_2} \tag{4}$$

subject to the minimum and maximum values of the design variables.

3.2. Sensitivity analysis

In most of the efficient optimization methods, the design sensitivity analysis is required to determine the derivatives of the objective functions with respect to the parameters of interest. In this paper we do not obtain the sensitivity derivatives explicitly from equations. Instead, the sensitivities of the natural frequencies of the suspension assembly to the design variables are numerically investigated. The purposes of plotting the sensitivity analysis are as follows:

(1) The designer may want to discard those design variables that are least sensitive to the natural frequencies.
(2) The designer may keep constants of those design variables to which the sensitivities are linear, or monotonic functions.
(3) Only the design variables that are not involved with the above two cases are retained for the subsequent optimal design.

In this way the number of the design variables can be kept minimal to expedite the design optimization of structures. On the other hand, decision makers can make a proper shift or modification of the final solutions according to the linearity of sensitivity with respect to a certain structural parameter.

In Figs. 4–6, the sensitivity curves of the first three natural frequencies are displayed with respect to a single

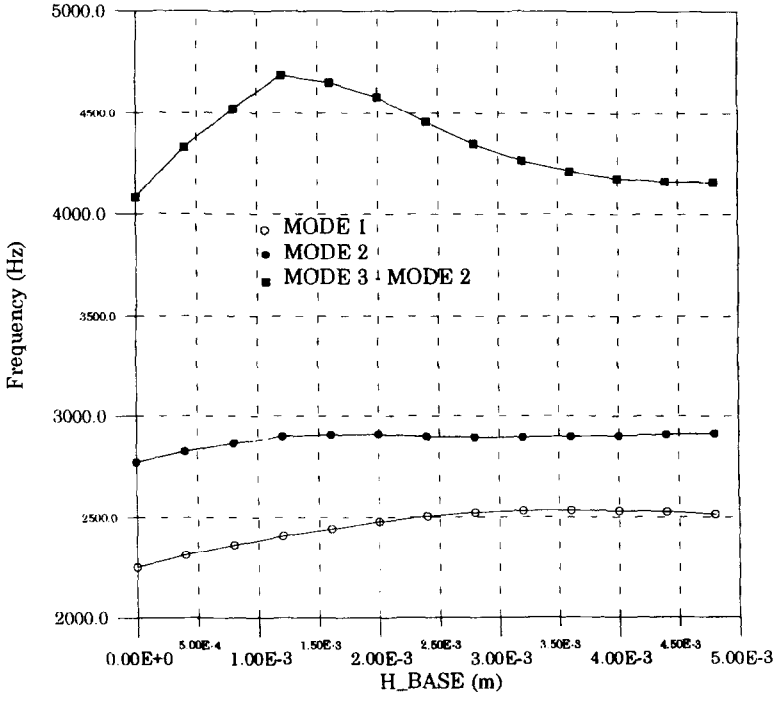

Fig. 4. Sensitivity of natural frequencies with respect to H_{BASE}.

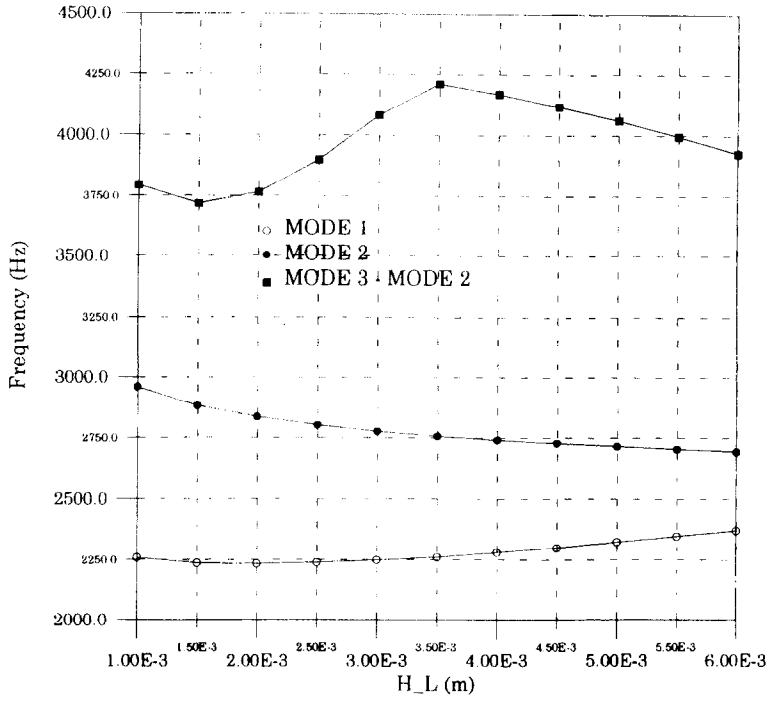

Fig. 5. Sensitivity of natural frequencies with respect to H_L.

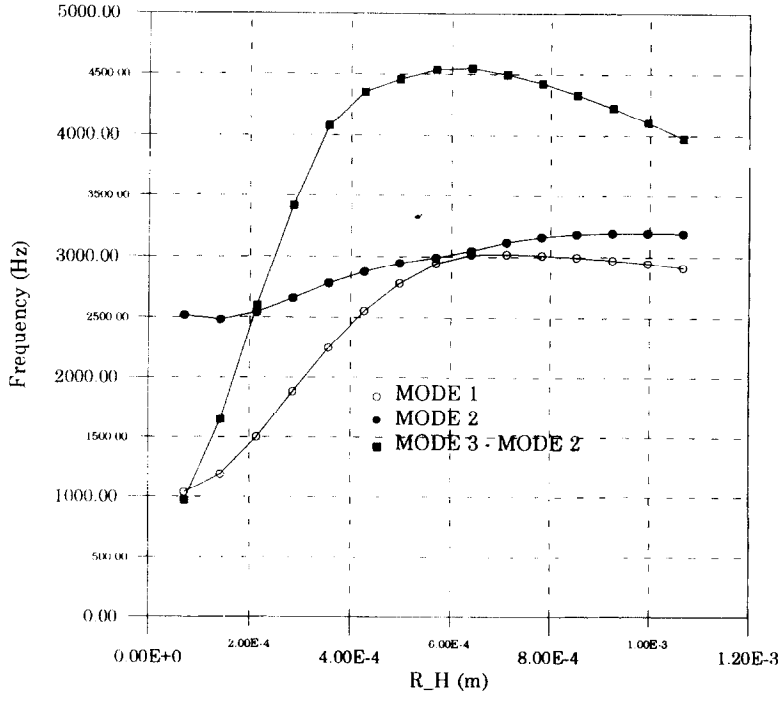

Fig. 6. Sensitivity of natural frequencies with respect to R_H.

design variable, while other design variables are fixed as the original values of the suspension assembly. Fig. 4 describes the sensitivity of the frequencies with the change of H_{BASE}, and shows that all the three curves have optimal values. It is true that a weak structure near the nodal line of a mode reduces the corresponding natural frequency. So, when the hole is located about the center of the suspension, away from the nodal line of the first mode, its natural frequency is a maximum. For a similar reason, the third mode has a maximum frequency when the hole is located between two nodal lines. As shown in Fig. 5 for the design variable H_L, the first natural frequency starts to increase slightly as the length of the hole increases, though the second (torsional) frequency decreases with a reduction of torsional stiffness. However, the third natural frequency apparently changes and has a maximum value in the range of the design variable. From Fig. 6, the natural frequencies are very sensitive to the height of suspension flaps, and can be increased greatly by the enlargement of the flap height in the current design.

Moreover, from a structural dynamics point of view, it is essential that the longer the suspension is, the smaller its natural frequencies are; and the thicker the suspension beam is, the larger its natural frequencies are. It is obvious that the natural frequencies of the suspension assembly vary monotonically with the thickness and length of the suspension, and they are not selected as design variables. Besides, the length and thickness of the suspension beam are usually determined by the restrictions on the size and space of the hard disk drives. Other design variables, such as H_{EDGE}, WE and $RAIL_A$, are not so sensitive to the natural frequencies that they are not chosen in the subsequent optimal design. The initial estimates of the design variables are listed in Table 2.

3.3. Integrated structure and control optimization

The design of actively controlled hard disk suspension assemblies must be formulated as a multiobjective optimization problem with integrated structure and control objectives. In terms of the vector of design variables $\boldsymbol{x}$, the Nth-order equations of motion (1) that describe the dynamic behavior of the suspension assembly can be transformed to principal (modal) coordinates

$$\ddot{\eta} + C'(\boldsymbol{x})\dot{\eta} + K'(\boldsymbol{x})\eta = B'(\boldsymbol{x})\boldsymbol{u} \tag{5}$$

using the matrix transformation

$$\boldsymbol{q} = \Phi(\boldsymbol{x})\eta \tag{6}$$

where η is the modal coordinate vector, and $\Phi(\boldsymbol{x})$ is the modal matrix whose columns are the corresponding normal modes, that is

$$\Phi(\boldsymbol{x}) = [\phi_1, \phi_2, \ldots, \phi_N]\,. \tag{7}$$

For simplicity, the argument $\boldsymbol{x}$ is omitted in subsequent analyses. The matrices K', C' and B' have been normalized, and represent the modal stiffness, modal damping, and modal input influence matrices, respectively, given by

$$K' = [\boldsymbol{m}]^{-1}\Phi^{\mathrm{T}}K\Phi = \mathrm{diag}(\omega_1^2 \quad \omega_2^2, \ldots, \omega_N^2) \tag{8}$$

$$C' = [\boldsymbol{m}]^{-1}\Phi^{\mathrm{T}}C\Phi = \mathrm{diag}(2\zeta_1\omega_1 \quad 2\zeta_2\omega_2, \ldots, 2\zeta_N\omega_N) \tag{9}$$

$$B' = [\boldsymbol{m}]^{-1}\Phi^{\mathrm{T}}B \tag{10}$$

in which

$$[\boldsymbol{m}] = \Phi^{\mathrm{T}}M\Phi = \mathrm{diag}(m_1, m_2, \ldots, m_N) \tag{11}$$

Table 2
Design parameters (mm)

Design variable	Original	Minimum	Maximum
H_{BASE}	2	0	5
H_L	3	1	6
R_H	0.356	0.1	1.2

is a diagonal modal mass matrix, ζ_i and ω_i are the damping ratio and natural frequency of the ith normal mode.

By the modal analysis the transformation to principal coordinates has uncoupled the equations of motion, leading to N separate single-degree-of-freedom equations. In fact, high-frequency modes possess less kinetic and potential energy, and decay much faster than low-frequency modes due to the structural damping. It is efficient and practical for the designer to truncate those modal coordinates that correspond to high-frequency modes. In the following optimal control formulation, 10 modal coordinates are selected which describe the dominant dynamic behavior of the suspension assembly. In state-space form, Eq. (5) is expressed as

$$\dot{\boldsymbol{y}} = \boldsymbol{A}\boldsymbol{y} + \boldsymbol{B}\boldsymbol{u} \tag{12}$$

where $\boldsymbol{y} = [\eta^{\mathrm{T}} \quad \dot{\eta}^{\mathrm{T}}]^{\mathrm{T}}$ is the state variable vector, and $\boldsymbol{A}$ and $\boldsymbol{B}$ are the plant and input matrices given by

$$\boldsymbol{A} = \begin{bmatrix} 0 & I \\ -K' & -C' \end{bmatrix} \quad \text{and} \quad \boldsymbol{B} = \begin{bmatrix} 0 \\ B' \end{bmatrix}. \tag{13}$$

In order to design a linear quadratic regulator, a performance index (PI) can be defined as

$$f_4 = \frac{1}{2}\int_0^{\infty} (\bar{\boldsymbol{q}}^{\mathrm{T}}\boldsymbol{Q}\bar{\boldsymbol{q}} + \boldsymbol{u}^{\mathrm{T}}\boldsymbol{R}\boldsymbol{u})\,\mathrm{d}t \tag{14}$$

where $\bar{\boldsymbol{q}} = [\boldsymbol{q}^{\mathrm{T}} \quad \dot{\boldsymbol{q}}^{\mathrm{T}}]^{\mathrm{T}}$, and $\boldsymbol{Q}$ and $\boldsymbol{R}$ are the state and control weighting matrices which must be positive semi-definite and positive definite, respectively. If the system is either uniformly completely controllable or exponentially stable, the minimization of the performance index for a set of design variables yields the steady-state optimal control law

$$\boldsymbol{u}^* = -\boldsymbol{R}^{-1}\boldsymbol{B}^{\mathrm{T}}\boldsymbol{P}\boldsymbol{y} \tag{15}$$

where $\boldsymbol{P}$ is the Riccati matrix that satisfies the algebraic equation

$$\boldsymbol{A}^{\mathrm{T}}\boldsymbol{P} + \boldsymbol{P}\boldsymbol{A} - \boldsymbol{P}\boldsymbol{B}\boldsymbol{R}^{-1}\boldsymbol{B}^{\mathrm{T}}\boldsymbol{P} + \boldsymbol{\Phi}_d^{\mathrm{T}}\boldsymbol{Q}\boldsymbol{\Phi}_d = 0 \tag{16}$$

in which $\boldsymbol{\Phi}_d = \mathrm{diag}(\Phi \quad \Phi)$. Therefore, the governing equation of the optimum closed-loop system can be written as

$$\dot{\boldsymbol{y}} = \bar{\boldsymbol{A}}\boldsymbol{y} \tag{17}$$

where

$$\bar{\boldsymbol{A}} = \boldsymbol{A} - \boldsymbol{B}\boldsymbol{R}^{-1}\boldsymbol{B}^{\mathrm{T}}\boldsymbol{P}. \tag{18}$$

The above optimal control formulation can be used in two ways. First, the optimal control analysis can be performed after the structure optimization is completed; that is, the optimal shape of the suspension assembly can be determined by minimizing the objective functions f_1, f_2 and f_3 defined in Eqs. (2)–(4), and then the control responses are obtained. Second, all the objective functions f_i, $i = 1$ to 4 can be considered simultaneously in the multiobjective optimization techniques of goal programming and compromise programming, as stated in Appendix B.

4. Optimization results

The optimization of the suspension assembly is investigated with two techniques: goal programming and compromise programming. The principles and solution procedures have been described [16]. These optimization algorithms are provided by MOST [17], in which the design variables, initial sizes of the suspension assembly, optimization techniques, objective functions, gradient calculation, and so on, are defined and coded in the C programming language. ABAQUS is called internally by MOST whenever a structural analysis for eigenvalues and eigenvectors is requested. The designer can either terminate the design loop for any feasible intermediate design, or wait for the final results. The interface between ABAQUS and MOST has been developed on a workstation under the UNIX operating system [18].

It is worth noticing that the minimum and maximum values of each objective function must be calculated

Table 3
Minimum/maximum values of objective functions and corresponding natural frequencies (Hz)

	Maximum value	Minimum value
f_1	7.87E-4	3.01E-4
f_2	4.42E-4	2.45E-4
f_3	3.07E-4	2.05E-4
f_4	1.3119	1.0487
ω_1	1270.5	3324.5
ω_2	2263.7	3802.4
$\omega_3 - \omega_2$	3253.3	4831.8

independently in the domain of the design variable space, as shown in Table 3, with the corresponding natural frequencies associated with each of the objectives. The weighting matrix $\boldsymbol{Q}$ in (14) is chosen as $10^{14}\boldsymbol{I}$ and $\boldsymbol{R} = 10$. The values of a set of design variables that lead to a minimum value of f_i^*, namely the *ideal solution* of each cost function f_i, are not always in the feasible region. Therefore, a best compromise solution is searched over all feasible solutions by minimizing their distances from the ideal solutions; thus the compromise between the objective functions yields an optimum.

4.1. Passive design and optimal control

The optimal design results of the suspension assembly obtained by the use of goal and compromise programming for β, $\gamma = 1$ and 2 are listed in Table 4. The optimal shapes in the finite element mesh for the case of $\beta = 1$ and $\gamma = 1$ are listed in Fig. 7.

It is interesting to note the order of the mode shapes changes: the first mode becomes a torsional mode, the second bending, and the third torsional. However, the results from the passive design on raising the natural frequencies are very satisfactory. First, with small manipulations of the three design variables, the first and second frequencies can be raised to 1000 Hz. Also, the difference between the second and third natural frequencies increases over the range 450 to 780 Hz. Second, the value of each objective function is larger than its minimum value and less than its maximum value as shown in Table 3. In other words, a nondominated solution, that results when a set of design variables minimize all the objectives, does not exist. Instead, an optimal solution is obtained by making compromises among the objective functions. Third, the suspension flap becomes about two times higher than in the original design, except for the compromise programming with $\gamma = 1$ with a smaller flap height. The designer must, therefore, consider the vertical dimension occupying the space between disks. This spacing will consider the slider height, baseplate height, loading clearance, suspension offset, arm thickness and flap height. The most common disk spacing when using the Type 870 suspension is 3.03 mm.

An optimal control system can be applied to the suspension assembly of a passive design. The optimal control system can be realized by adhering a piezoelectric material to the surface of the suspension assembly to produce

Table 4
Passive design variables (mm) and natural frequencies (Hz)

	$\beta = 1$	$\beta = 2$	$\gamma = 1$	$\gamma = 2$
H_{BASE}	1.922	1.895	1.476	1.562
H_L	3.092	3.458	1.441	2.272
R_H	0.601	0.614	0.691	0.723
f_1	3.05E-4	3.04E-4	3.01E-4	3.01E-4
f_2	2.69E-4	2.65E-4	2.75E-4	2.68E-4
f_3	2.19E-4	2.22E-4	2.07E-4	2.13E-4
ω_1	3281.5	3285.3	3320.6	3318.3
ω_2	3712.9	3764.9	3631.5	3729.9
$\omega_3 - \omega_2$	4574.1	4503.3	4826.2	4688.2

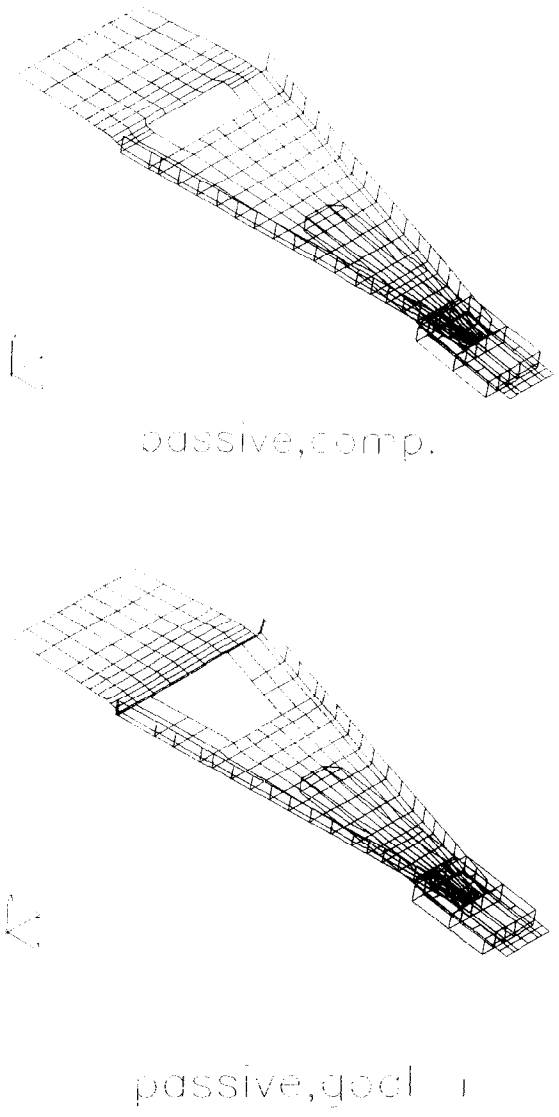

Fig. 7. Passive design results. (a) Goal programming ($\beta = 1$); (b) compromise programming ($\gamma = 1$).

an actuating force in the z-direction. This constrains the vertical control force to the centerline of the suspension, which is the nodal line of a torsional mode. Fig. 8 shows the closed-loop frequency responses of a passively designed suspension assembly. It is not surprising that all the bending modes are suppressed by the vertical force. However, the torsional modes cannot be controlled by the vertical force. These frequency responses were simulated by the action of external excitations, in all the six degrees of freedom, near the center of the suspension system that was approximated by the first six modes of the optimal shape. The displacement of the read/write head was measured as an output.

4.2. Active design with optimal vertical control

For the active design, we integrated the passive structure design objectives with an optimal control performance index; i.e. the objective functions f_1, f_2, f_3 and f_4 are simultaneously considered in the optimization. The same control effort is implemented independently in the z-direction as stated in the above section. Table 5 shows the final values of the design variables, natural frequencies and the corresponding costs. The optimal shapes in the finite element mesh for the case of $\beta = 1$ and $\gamma = 1$ are presented in Fig. 9.

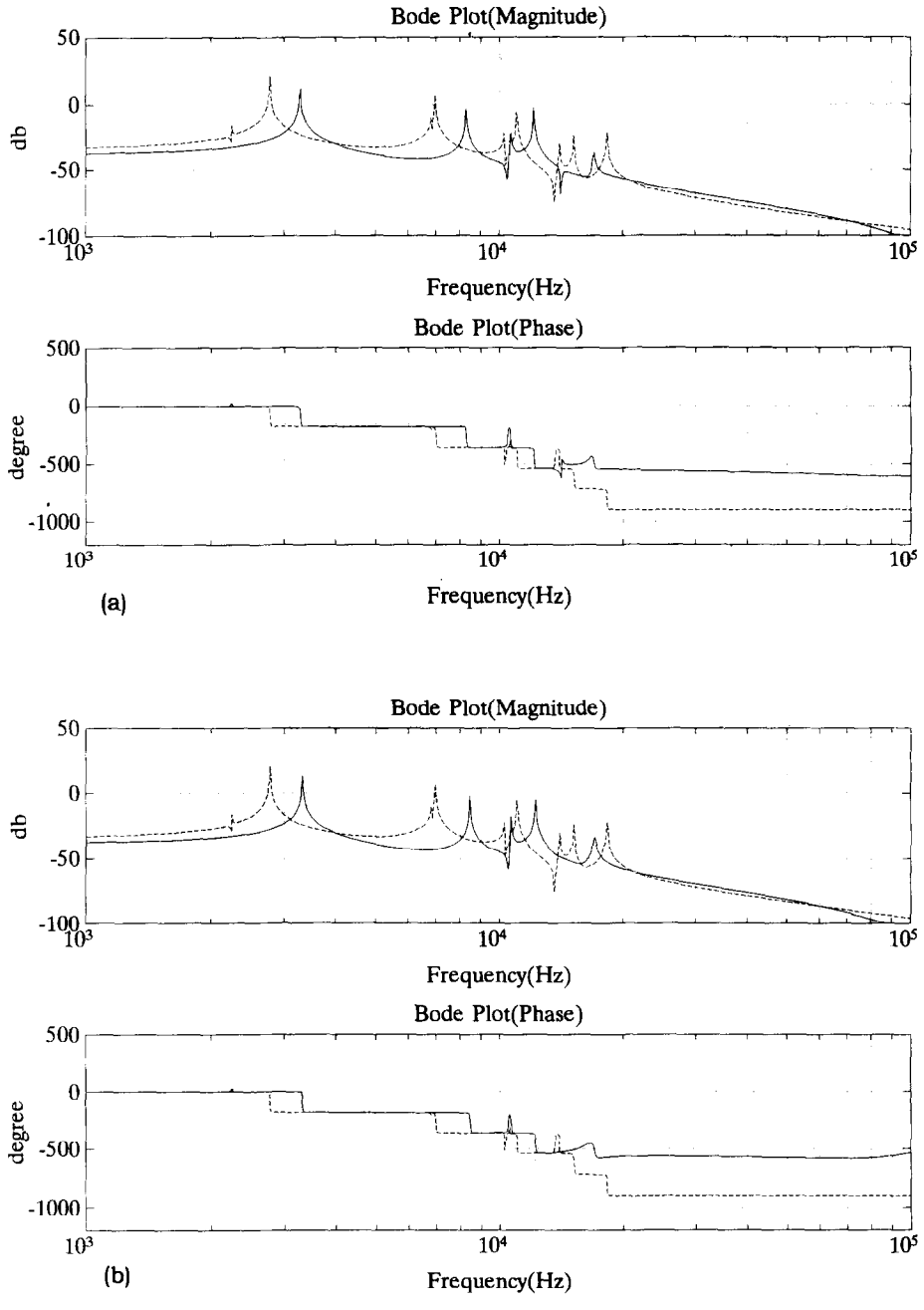

Fig. 8. Closed-loop frequency response of suspension by passive design. (a) Goal programming ($\beta = 1$, solid curve); (b) compromise programming ($\gamma = 1$, solid curve) (dashed curves: original suspension).

The final results on raising the natural frequencies are still satisfactory, though the first natural frequency is not raised as high as that in the passive design. This is reasonable since the additional cost of f_4 relatively reduces the weighting, or the importance, of the objectives f_i, $i = 1, 2, 3$. From the Bode plots of Fig. 10, we see that based on the design from the goal and compromise programmings, the bending modes, i.e. the first and third modes, are successfully restrained. However, the torsional modes cannot be controlled because the control force is perpendicular to the surface of the suspension and is on the nodal line of the torsional modes.

Table 5
Active design variables (mm) and natural frequencies (Hz): of the vertical optimal control design

	$\beta = 1$	$\beta = 2$	$\gamma = 1$	$\gamma = 2$
H_{BASE}	1.041	1.035	1.100	1.090
H_1	5.985	5.995	6.000	5.989
R_H	1.200	1.200	1.200	1.200
f_1	3.251E-4	3.251E-4	3.238E-4	3.238E-4
f_2	2.71E-4	2.70E-4	2.69E-4	2.70E-4
f_3	3.02E-4	3.02E-4	3.02E-4	3.02E-4
f_4	1.2270	1.2280	1.2198	1.2199
ω_1	3076.1	3074.9	3088.2	3088.2
ω_2	3691.1	3689.7	3710.1	3709.7
$\omega_3 - \omega_2$	3310.2	3308.0	3309.7	3311.6

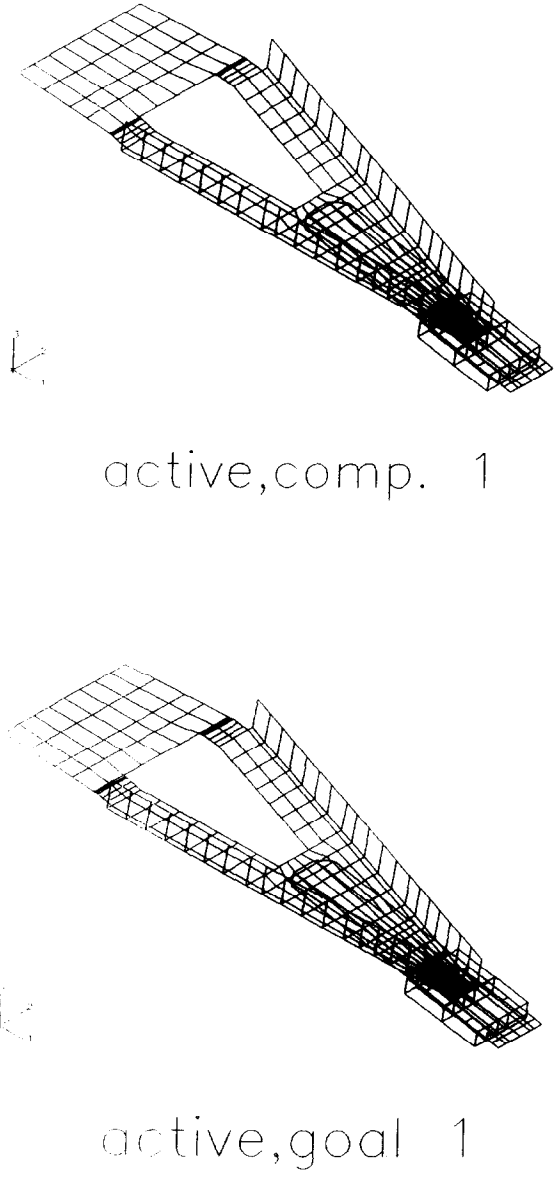

Fig. 9. Active design with vertical control. (a) Goal programming ($\beta = 1$); (b) compromise programming ($\gamma = 1$).

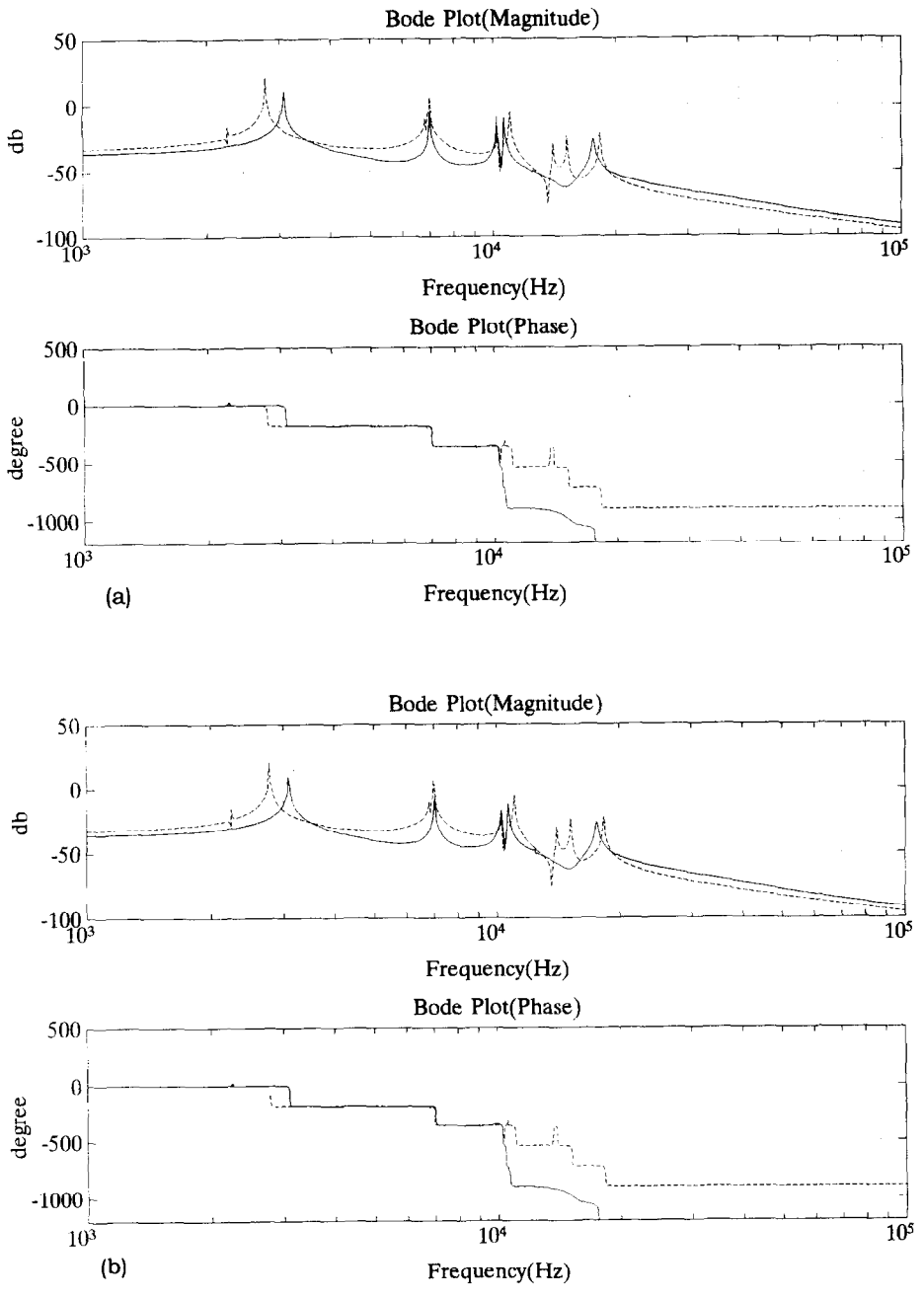

Fig. 10. Closed-loop frequency response of suspension by active design with vertical control. (a) Goal programming ($\beta = 1$, solid curve); (b) compromise programming ($\gamma = 1$, solid curve) (dashed curves: original suspension).

4.3. Active design with both vertical and lateral control efforts

The torsional modes are not controllable by a control force at the centerline line and perpendicular to the surface of the suspension. However, a lateral control force, which is parallel to the surface of the suspension, is able to suppress the torsional vibrations. It is then adequate to implement the control forces independently in both the y and z-directions on the yz-plane. This control system can be realized by the use of piezoelectric

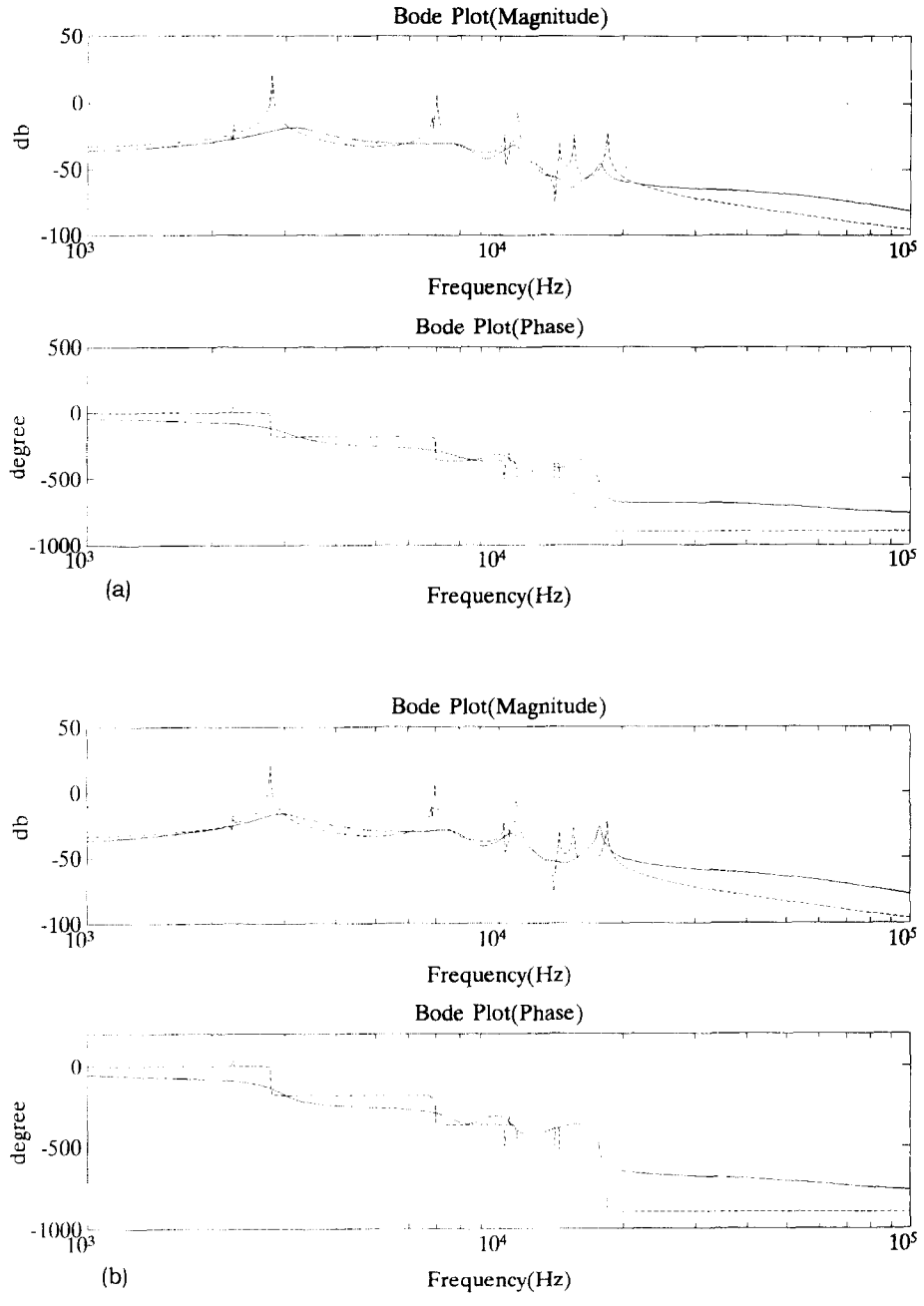

Fig. 11. Closed-loop frequency response of suspension by active design with vertical and lateral control. (a) Goal programming ($\beta = 1$, solid curve); (b) compromise programming ($\gamma = 1$, solid curve) (dashed curves: original suspension).

actuators with orthogonal control directions [19,20]. Fig. 11 shows the Bode plots of the active design obtained by the goal and compromise programming, respectively, with independent control forces in the y and z-directions. These closed-loop frequency responses reveal that all the bending and torsional modes are perfectly suppressed. Table 6 shows the corresponding values of design variables, natural frequencies and costs. The optimal shapes in the finite element mesh for the case of $\beta = 1$ and $\gamma = 1$ are presented in Fig. 12.

Table 6
Active design variables (mm) and natural frequencies (Hz): vertical and lateral optimal control

	$\beta = 1$	$\beta = 2$	$\gamma = 1$	$\gamma = 2$
H_{BASE}	1.370	1.370	1.370	1.434
H_L	6.000	6.000	6.000	6.000
R_H	0.463	0.470	0.393	0.413
ω_1	3052.1	3064.8	2911.4	2957.4
ω_2	3483.5	3512.8	3166.1	3272.8
$\omega_3 - \omega_2$	4174.2	4160.1	4435.5	4276.8
COST	2.4167	2.4271	2.3312	2.3854

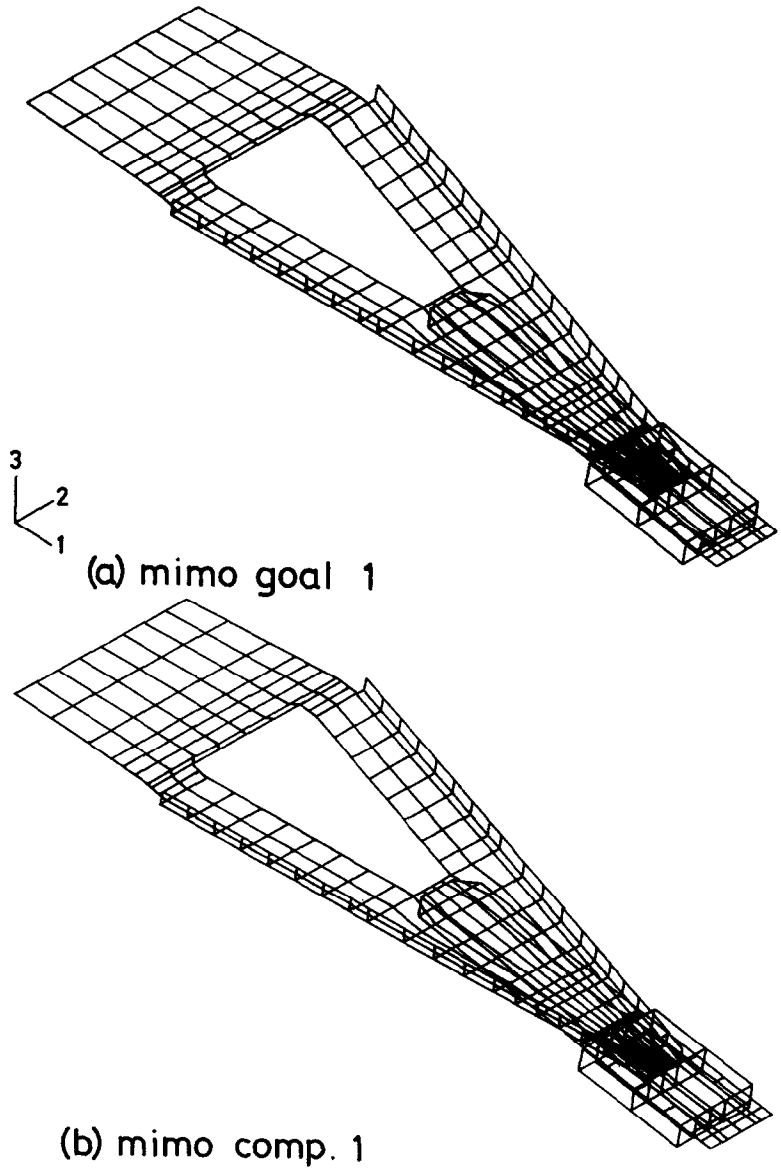

Fig. 12. Active design with vertical and lateral control. (a) Goal programming ($\beta = 1$); (b) compromise programming ($\gamma = 1$).

5. Summary and conclusions

A multiobjective optimization design methodology for the suspension assembly of hard disk drives has been presented. The passive design deals with the optimization of the natural performance of the suspension structure. The primary design objective is to maximize the natural frequencies of the suspension assembly to reduce the excitation caused by undesirable disturbances. The active design seeks to control the additional parameters of weighted system state regulation errors and control efforts, and is therefore called the integrated structure/control multiobjective optimization design. Both the goal programming and compromise programming techniques give feasible solutions, which though not ideal, are the optimal in the sense that they represent a best compromise among objectives. The appropriate choice of a control system requires investigation of the closed-loop frequency and time responses. Although both the passive and active designs present satisfactory results, an additional lateral force control on the optimal shape is clearly helpful in controlling the torsional modes. The final solution may not be unique, but will depend on a combination of factors including the engineering experience level of the design team, and the manufacturing requirements.

Acknowledgment

This research was supported by National Science Council under Contract No. NSC85-2212-E-002-057.

Appendix A. Original dimensions of suspension beam, flexure and slider

A. Suspension Beam, Flexure and Slider (unit: **mm and degrees**)

WE	0.899	WM	5.960	$WM1$	6.370	WMX	5.090
WB	5.320	H_{EDGE}	1.270	H_{BASE}	2.000	E_{WELD}	0.780
H_W	3.180	H_L	3.000	$L1$	12.71	$L2$	5.330
$L3$	2.440	$L4$	0.780	$WELD1$	11.54	$WELD2$	13.90
$WELD3$	15.63	R_H	0.356	FX_1	2.000	$FXCL$	3.660
$FXW1$	1.170	$FXW2$	1.190	$FXW3$	2.920	FY	0.953
FXR	7.820	$TORQUE_L$	3.530	FWY	0.480	$CONNECT_W$	0.333
$Slider_l$	3.180	$Slider_w$	2.264	$Slider_h$	0.660		

$E = 2.0601 \times 10^{11}$ Nm^2 (Young's modulus).
Suspension material thickness = 0.076 mm.
Flexure material thickness = 0.0381 mm.
$d = 7.8 \times 10^3$ kg/m^3 (density).
$\mu = 0.33$ (Poisson ratio).

Appendix B. Multiobjective optimization algorithms in MOST

B.1. Goal Programming

The objective of goal programming is to minimize the difference between the optimal solution and the ideal solution in the objective function space. The difference between these functions is represented by the under-achievement and over-achievement of the ith objective function $f_i(\boldsymbol{x})$, defined respectively by

$$d_i^+ = 0.5[|f_i(\boldsymbol{x}) - T_i^*| + (f_i(\boldsymbol{x}) - T_i^*)] \geq 0 \tag{B.1}$$

$$d_i^- = 0.5[|f_i(\boldsymbol{x}) - T_i^*| - (f_i(\boldsymbol{x}) - T_i^*)] \geq 0 \tag{B.2}$$

where T_i^* represents the target or goal set by the decision maker for the ith objective function. The general formulation for nonlinear optimization problems can be stated as [21]:

$$\min F(x) = \left\{ \sum_{i=1}^{q} (d_i^+ + d_i^-)^\beta \right\}^{1/\beta} \quad ; \quad \beta \geq 1 \tag{B.3}$$

subject to the constraints

$$h_j(x) = 0 \; ; \quad j = 1, 2, \ldots, p$$

$$g_j(x) \leq 0 \; ; \quad j = 1, 2, \ldots, m$$

$$T_i(x) = f_i(x) - d_i^+ + d_i^- \; ; \quad i = 1, 2, \ldots, q$$

in which the value of β is based on the utility function chosen by the decision maker. Nondominated solutions can be obtained by varying the values of β and T_i.

B.2. Compromise Programming

The compromise programming [22] seeks to minimize the distance between the ideal solution and the optimal solution resulting in a so-called *compromise solution*. The distance measure used in compromise programming, which evaluates how close the set of nondominated points come to the ideal point is the family of L_γ matrices defined as

$$\min L_\gamma = \left\{ \sum_{i=1}^{q} \alpha_i^\gamma \left| \frac{f_i(x) - f_i^*}{f_{i,\max} - f_i^*} \right|^\gamma \right\}^{1/\gamma} \quad ; \quad 1 \leq \gamma < \infty \tag{B.4}$$

subject to $x \in X$, in which α_i are weights, f_i^* and $f_{i,\max}$ are, respectively, the minimum value and the worst value of the ith objective function, $f_i(x)$ is the value of implementing the design variable x with respect to the ith objective, and X is the feasible design space.

In the case of $\gamma = 1$, all deviations from f_i^* are taken into consideration in proportion to their magnitudes. For $2 \leq \gamma < \infty$, the larger the deviation, the larger the weight in L_γ. In the limiting case of $\gamma = \infty$ only the largest deviation from the minimum objectives is considered.

References

[1] R.D. Cormia and D. Mann, Contact recording on rigid disks: Materials and materials analysis, Solid State Tech. (1992) 59–61.

[2] J. Naruse, M. Tsutsumi, T. Tamura, Y. Hirano, T. Hayama and O. Matsushita, Design of a large capacity disk drive with two actuators, IEEE Trans. Magn. 19 (1983) 1695–1697.

[3] Y. Yamaguchi, A.A. Talukder, T. Shibuya and M. Tokuyama, Air flow around a magnetic-head-slider suspension and its effect on slider flying-height fluctuation, IEEE Trans. Magn. 26(5) (1990) 2430–2432.

[4] M. Takuyama, Y. Yamaguchi, S. Miyata and C. Kato, Numerical analysis of flying-height fluctuation and positioning error of magnetic head due to flow induced by disk rotation, IEEE Trans. Magn. 27(6) (1991) 5139–5141.

[5] O.G. McGee and K.F. Phan, A robust optimality criterion procedure for cross-sectional optimization of frame structures with multiple frequency limits, Comput. Struct. 38(5/6) (1991) 485–500.

[6] W. Szyszkowski and J.M. King, Optimization of frequencies spectrum in vibrations of flexible structures, AIAA J. 31(11) (1993) 2163–2168.

[7] R. Grandhi, Structural optimization with frequency constraints—A review, AIAA J. 31(12) (1993) 2296–2303.

[8] R.A. Canfield, High-quality approximation of eigenvalues in structural optimization, AIAA J. 28(6) (1990) 1116–1122.

[9] W. Szyszkowski, Multimodal optimality criterion for maximum fundamental frequency of free vibrations, Comput. Struct. 41(5) (1991) 909–916.

[10] E. Livne, L.A. Schmit and P.P. Friedmann, Integrated structure/control/aerodynamics synthesis of actively controlled fiber composite wings, J. Aircraft 30(2) (1993) 387–394.

[11] M.G. Gilbert and D.K. Schmidt, Integrated structure/control law design by multilevel optimization, J. Guidance 14(5) (1991) 1001–1006.

[12] S.S. Rao, Multiobjective optimization of actively controlled structures, Proceedings of the 11th Conference on Analysis and Computation (Atlanta, GA, 1994) 276–285.

[13] L.J. Pan, The control of slider flying height fluctuation in a hard disk, Master's Thesis, Department of Mechanical Engineering, National Taiwan University, ROC, 1993.

[14] S. Yoneoka, T. Owe, K. Aruga, T. Yamada and M. Takahashi, Dynamics of inline flying-head assemblies, IEEE Trans. Magn. 25(5) (1989) 3716–3718.

[15] F. Szidarovszky, M.E. Gershon and L. Duckstein, Techniques for Multiobjective Decision Making in System Management (Elsevier Science Publishing Co., New York, 1986).
[16] C.H. Tseng, T.W. Lu and L.W. Wang, Multiobjective optimization with non-continuous design variables, J. Chinese Soc. Mech. Engrs. 13(6) (1992) 547–560.
[17] C.H. Tseng, W.C. Liao and T.C. Yang, MOST User's Manual Version 1.1, Technical Report No. AODL-93-01 National Chiau-Tung University, Taiwan, ROC, 1993.
[18] Y.P. Yang and C.H. Tseng, Multiobjective optimization of complex structures integrated with finite element software on workstations, J. Chinese Soc. Mech. Engrs. 16(2) (1995) 167–179.
[19] K. Mori, T. Shimizu, T. Masukawa and T. Takahashi, Experimental evaluation of a head assembly by using a piezoelectric tripod shaker, IEEE Trans. Magn. 29(6) (1993) 3921–3923.
[20] V.K. Varadan, S.Y. Hong and V.V. Varadan, Piezoelectric sensors and actuators for active vibration damping using digital control, IEEE Ultrasonic Symp. (1990) 1211–1214.
[21] G.W. Evans, An Overview of techniques for solving multiobjective mathematical programs, Mgmt. Sci. 30(11) (1984) 1268–1282.
[22] M. Zeleny, Multiple Criteria Decision Making (McGraw-Hill, New York, 1982).